Journal of Biomedical Materials Research Part A

WILEY

Society For Biomaterials

RESEARCH ARTICLE OPEN ACCESS

Investigating the Effect of Thickener Concentrations on the Corrosion Behavior of Pure Mg

Manas Ranjan Sahu | Akiko Yamamoto

Research Centre for Macromolecules and Biomaterials, National Institute for Materials Science, Ibaraki, Japan

Correspondence: Manas Ranjan Sahu (sahu.manasranjan@nims.go.jp)

Received: 18 September 2024 | **Revised:** 24 December 2024 | **Accepted:** 9 January 2025

Funding: This work was supported by Japan Society for the Promotion of Science and Ministry of Education, Culture, Sports, Science and Technology.

Keywords: biodegradable metals | electrochemical impedance spectroscopy | in vitro model tissue | Potentiodynamic polarization | pure Mg

ABSTRACT

Magnesium (Mg) and its alloys are promising biodegradable implant materials due to their biocompatibility and ease of corrosion in physiological environment. In the tissue, diffusion of ions and gas released by Mg corrosion reaction will be interfered by extracellular matrix and cells, which may retard the corrosion reaction. Therefore, in the present study, we developed the in vitro model tissue with different diffusion rates to understand the effect of diffusion on the Mg corrosion. A thickener called gellan gum was added to the cell culture medium at appropriate concentrations to simulate tissues with different diffusion rates. The immersion study up to 28 days and the electrochemical studies were performed to evaluate the Mg corrosion behavior. The pure Mg specimens without thickener showed the highest corrosion rate in both immersion and electrochemical tests. The highest amount of insoluble salt layer with the lowest Mg and highest O concentrations were deposited on the specimen surface without thickener. The microfocus X-ray computed tomography (μCT) analysis confirmed these findings, showing the lowest remaining volume for specimens without thickener. There is an impediment of ion diffusion in the model tissue with increased thickener concentrations, thereby decreasing the corrosion rate. The corrosion rate for 0.2–0.3 wt. % thickener matched in the range of reported in vivo results. Hence, this model proves to be an effective tool for investigating biodegradation and understanding the mechanisms and controlling factors of this phenomenon.

1 | Introduction

Magnesium (Mg) and its alloys have received considerable attention as biodegradable implant materials because of their excellent biocompatibility and easiness to be corroded in the physiological environment [1, 2]. Mg is an essential mineral for the human body, with a concentration of 2.1 mEq/L in normal human serum [3] therefore compounds of released Mg^{2+} are non-toxic. Mg plays a crucial role in numerous physiological activities, including the regulation of more than 300 enzymes, blood pressure control, protein synthesis, structural development of bone, cellular energy metabolism, etc. [3].

The high electrode potential of Mg leads to its reaction with H_2O in the body fluid and resulted in too fast corrosion with excessive evolution of H_2 gas. The faster corrosion rate leads to loss in the mechanical integrity of the implant with the occurrence of tissue and implant failure at the early stage of the healing process [4, 5]. The excess H_2 gas evolved during the corrosion process accumulates in the surrounding tissue as gas cavities resulting in tissue layer separation [6]. Therefore, it is essential to have a controlled corrosion rate of Mg for its successful use as temporary implant applications.

To evaluate the corrosion rate of Mg and its alloys for their medical applications, various in vitro immersion-based evaluations such as static, semi-static, and dynamic corrosion tests were employed in the laboratory. However, the corrosion rates observed in vivo are generally lower than those measured in vitro [7–13]. Furthermore, the microenvironment of the implantation site and individual

conditions (such as age, underlying diseases, etc.) also cause variations in the resulting corrosion rate [8, 14]. Therefore, estimation of the corrosion rate of Mg and its alloys in the physiological environment by an in vitro test is a challenging task.

Currently, no systematic approach has been established regarding the experimental conditions necessary to study Mg corrosion that adequately bridges the gap between in vitro results and in vivo performance. The observed discrepancies highlight the need to optimize in vitro test designs to more accurately reflect in vivo conditions, thereby reducing the necessity for animal experiments. Various factors such as inorganic ions, organic compounds, pH, etc. influence the corrosion rate of Mg [12, 15]. Among these, one of the most critical environmental factors affecting the corrosion rate in vivo is the diffusion rate of ions and gasses through the tissue [13, 14]. In vivo, the extracellular matrix and cells in the tissue hinder the diffusion of ions and gas released by the Mg corrosion. Therefore, it is necessary to consider the diffusion effect in designing the in vitro test.

To understand the effect of diffusion on Mg corrosion, in our previous studies, a model tissue was developed by the addition of a thickener to the cell culture medium to reduce the diffusion rate in the corrosion environment [16, 17]. However, these studies were limited to analyzing the insoluble salt layer (ISL) precipitation after 7 days of immersion and gas cavity formation over 28 days. These preliminary findings indicate the need for a detailed investigation of the effect of thickener concentrations on the corrosion behavior of Mg.

The objective of the current study is to evaluate the influence of different thickener concentrations on the corrosion behavior of Mg. The immersion test for up to 28 days and the electrochemical test including both electrochemical impedance spectroscopy (EIS) and potentiodynamic polarization (PDP) tests were performed to evaluate the corrosion behavior in detail. Additionally, the mechanical properties of the model tissue were also evaluated by performing the compression test.

2 | Experimental Procedure

2.1 | Sample Preparation

A commercially available pure Mg rod with 9.5 mm in diameter and 300 mm in length (99.95%, impurities of 0.005% Zn, 0.032% Al, 0.016% Si, 0.001% Cu, 0.015% Mn, 0.006% Fe, and 0.001% Ni) was obtained via Nilaco Corporation, Japan. The disks of 2 mm in thickness were cut from the rod and polished with #600 SiC paper. After polishing, the specimens were cleaned with ethanol and air-dried. In prior to the immersion test, the specimens were sterilized by ethylene oxide gas (EOG) and stored in vacuum.

2.2 | Model Tissue Preparation

To prepare the model tissue, a polysaccharide thickener (gellangum, FUJIFILM Wako Pure Chemical Corporation) was added to the cell culture medium (Eagle's minimum essential medium supplemented with 10 vol. % newborn bovine serum, abbreviated as E-MEM + NBS) to form a gel to reduce the diffusion rate in the corrosion environment [16, 17]. No cells are involved for the simplicity and easiness in preparation. The thickener concentrations of 0.1%, 0.2%, and 0.3% were employed to mimic different diffusion rates in the tissue. As a control, E-MEM + NBS was used. The preparation procedures are briefly described as follows. An appropriate amount of the thickener was dissolved in Milli-Q water at 90°C, followed by the addition of an appropriate amount of 10 times concentrated E-MEM (AccuDia Eagle's MEM①) solution. After sterilization by autoclaving, L-glutamine, $NaHCO_3$, and NBS were aseptically added. Then, it was kept in an incubator at 51° ± 1°C under the atmosphere of 5% CO_2 in a humidified air for overnight to adjust its pH while maintaining its solution state. The prepared solution with the thickener was poured into a glass vessel with/without a specimen and placed in an CO_2 incubator at 37° ± 1°C which allows gelation.

A compression test of the model tissue was performed to examine the effect of the thickener on its mechanical properties. An appropriate amount of the pre-incubated model tissue solution with the thickener concentration of 0.1%, 0.2%, or 0.3% was poured into a flat-bottom glass vessel with 40 mm in diameter to form the gel with 15 mm in depth. The dishes were placed in a CO_2 incubator at 37° ± 1°C for 24 h to allow gelation. Then, the model tissue in the flat-bottom vessel was compressed by the plunger of 20 mm in diameter at the speed of 1 mm/s up to the clearance of 5 mm from the bottom of the vessel using a texture analyzer (FRTS-5N, IMADA Co. Ltd.). The compression rate was selected based on the testing condition for Jelly strength in Japanese Industrial standard JIS K6503:2001. Measurement was performed at 20° ± 2°C with a constant time interval after taking the vessel out from the CO_2 incubator. The compression modulus was decided as the initial slope of the stress–strain curve obtained.

2.3 | Immersion Test

A sterilized specimen was placed in the bottom of a glass dish (60 mm in diameter) and an appropriate amount of the pre-incubated model tissue solution was poured over it. The volume of the solution was selected to be 15 mL/cm^2 of the whole specimen surface. Then, the dishes were placed in a CO_2 incubator at 37° ± 1°C for 7, 14, or 28 days.

After the immersion, the collected specimens were dried in vacuum and inspected using an optical microscope (SZ60, Olympus Corporation). The deposits on the specimen surface were analyzed by X-ray fluorescence spectroscopy (XRF, ZSX Primus2, Rigaku Corporation) by the EZ scan mode for metal samples at 4 kW with the analyzing area of 10 mmϕ.

The microfocus X-ray computed tomography (μCT) observation was performed at 90 kV and 110 μA using SMX-90CT (Shimadzu Corporation) with the resolution of 11 μm/voxel. The remaining volume of the specimen was calculated based on the obtained images using an image analysis software (VGStudio MAX3.0, Volume Graphics GmbH).

Finally, a chromic acid solution [20 g CrO_3, 1 g of $AgNO_3$, and 2 g of $Ba(NO_3)_2$ dissolved in 100 mL of Milli-Q water] was employed for the removal of ISL. After acid cleaning, the specimens were rinsed with Milli-Q water and dried in vacuum. The weight of

the specimens after drying were measured and the weight loss per unit surface area was calculated using the following equation:

$$\Delta W = \frac{W_b - W_a}{S_b} \quad (1)$$

where ΔW is the weight loss per unit surface area (in mg/cm^2), W_b and W_a are the weight before immersion and after acid cleaning (in mg), and S_b is the initial surface area of the specimen (in cm^2).

2.4 | Electrochemical Test

A typical three-electrode system consisting of a platinum wire as the counter electrode, Ag/AgCl (3 M NaCl) as the reference electrode, and the specimen (exposed area of 0.332 cm^2) as a working electrode, was used. A Mg specimen was set on the bottom of an electrochemical chamber, followed by addition of the 5 mL portion of the pre-incubated model tissue solution or E-MEM + NBS. Electrochemical measurements were performed in the incubator (37° ± 1°C, 5% CO_2 in humidified air) with a potentiostat equipped with a frequency response analyzer (VersaSTAT4, Princeton Applied Research). After incubation of 2, 6, 12, and 24 h, EIS was measured at the open circuit potential (OCP) with alternating current (AC) amplitude of 5 mV in the frequency range of 10^{-2}–10^5 Hz. PDP was performed after 24 h of incubation at a scanning rate of 0.5 mV/s with the potential range from −0.25 V vs. OCP to that giving the current density over 1 mA/cm^2. EIS data was analyzed with an equivalent circuit model using the Zview software (version 4.0f, Scribner Associates Inc.). PDP data was analyzed by the VersaStudio software (version 2.66.2, Princeton Applied Research). The specimens collected after the electrochemical test were observed by scanning electron microscopy (FE-SEM S-4800, Hitachi High-Tech Corporation).

2.5 | Statistical Analysis

All the data are presented as mean ± standard deviation (SD). Statistical analysis was performed by one-way ANOVA together with a multi-comparison by Tukey test (Kyplot 6.0, KyensLab Inc.). A probability of p-value < 0.05 was considered statistically significant.

3 | Results

3.1 | Compression Modulus of the Model Tissue

The stress–strain curves obtained from the compression test of different model tissues are shown in Figure 1. The ultimate stress increased with the increase in thickener concentrations of the model tissue. The modulus of model tissue with 0.1%, 0.2%, and 0.3% thickener were 308.4 ± 12.1, 1602.6 ± 17.7, and 3429.0 ± 98.9 Pa, respectively. They are plotted against the thickener concentrations as shown in Figure 1b, indicating the increase in compression modulus with the increase in the thickener concentration.

3.2 | Immersion test

3.2.1 | Morphology of the Insoluble Salts on the Specimen Surface

Figure 2 shows the surface morphology of the pure Mg specimens after the immersion test for different time periods. The amount of ISL deposited on the specimen surface increased with the increase in immersion time for all the thickener concentrations. The specimens immersed in E-MEM + NBS had the most dense ISL deposition in all the immersion periods indicating the highest corrosion rate in E-MEM + NBS among the conditions tested. After 7 and 14 days of immersion, the specimens immersed in the model tissue with 0.1% thickener had no obvious insoluble salt deposition, whereas the specimens immersed in 0.2% and 0.3% thickener had some ISL. After 28 days, the specimens immersed in 0.1% thickener showed uniform deposition of ISL on its surface, whereas those in 0.2% and 0.3% thickener showed non-uniform deposition of ISL.

3.2.2 | Elemental Analysis of the Specimen Surface

The results of XRF analysis are shown in Figure 3 and Supplementary Table S1. At all the immersion periods, the specimens immersed in E-MEM + NBS had the lowest Mg and the highest O concentrations than those immersed in the

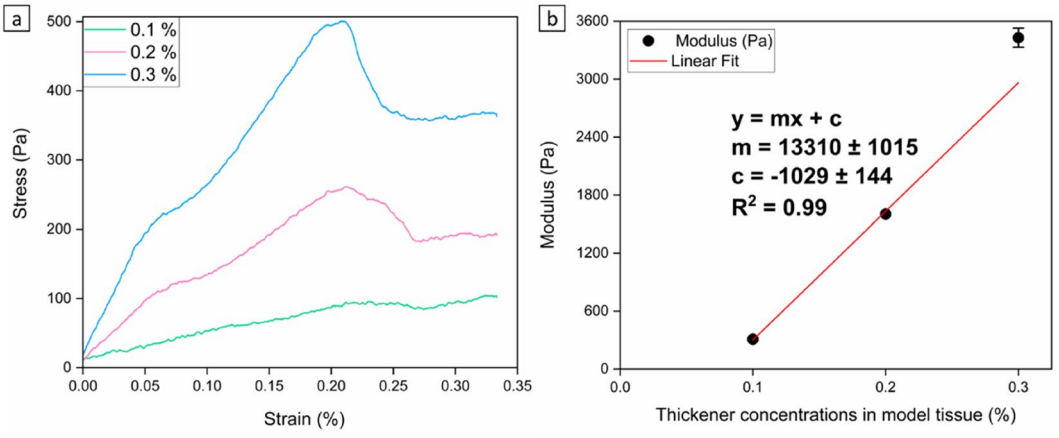

FIGURE 1 | (a) The stress vs. strain curve and (b) the compression modulus of model tissue with various thickener concentrations ($n = 3$).

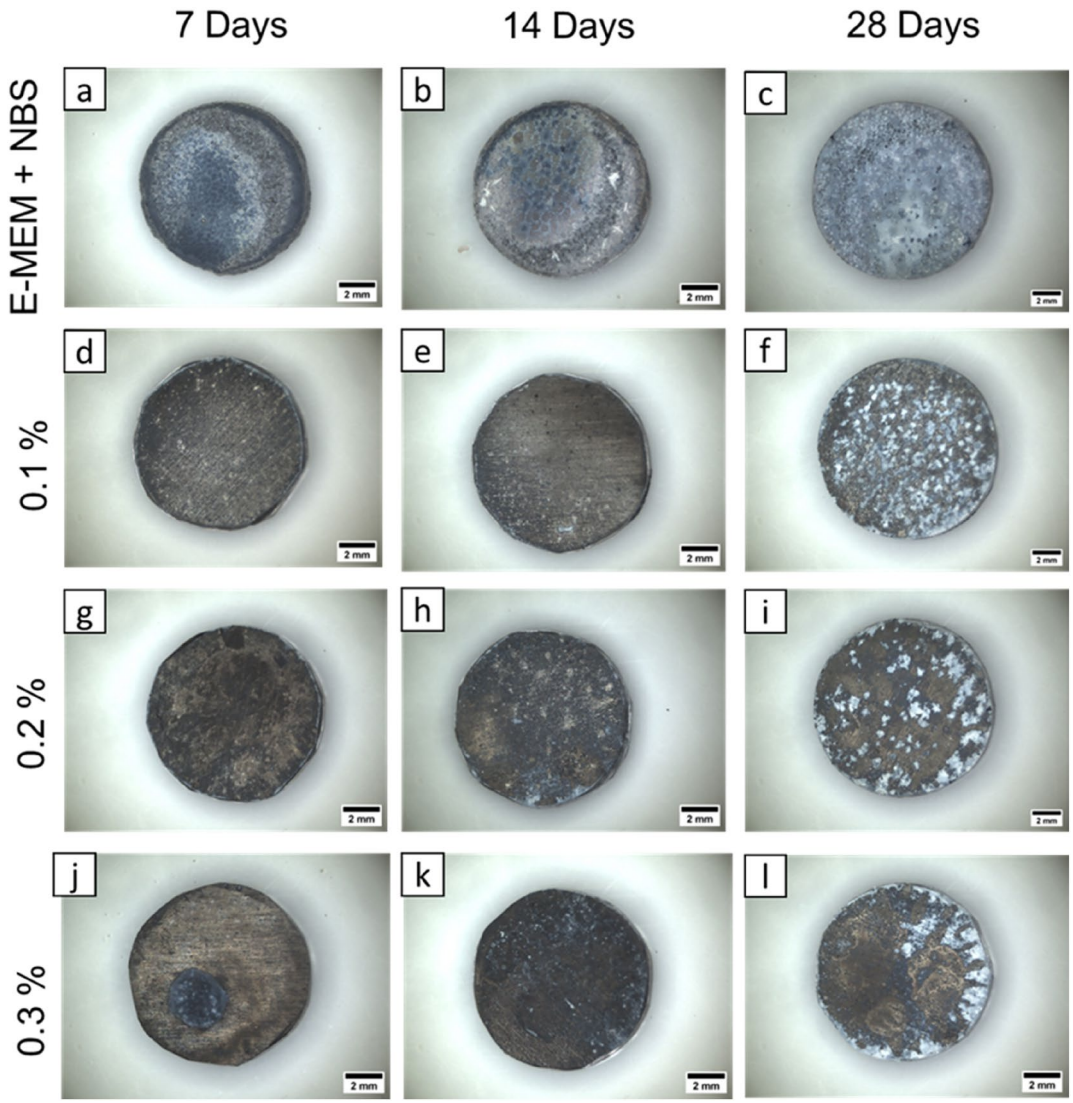

FIGURE 2 | The optical microscopic observation of the pure Mg specimens after the immersion test ($n = 3$).

model tissue with thickeners. This agrees with the thick ISL observed in Figure 2 and indicates the highest corrosion rate in E-MEM + NBS. With the progress in the immersion period, there is a decreasing trend in the Mg concentration and an increasing trend in the O concentration for all the specimens in model tissues with thickener, indicating the progress of the ISL formation on the specimen surface with time. Most of the specimens had an increasing trend in concentrations of Ca and P from 7 to 28 days (Table S1). The increase in Ca concentration is more obvious for the specimens immersed in E-MEM + NBS than those immersed in model tissue with thickener.

3.2.3 | Volume Loss Based on the μCT Images

The remaining volume of the specimens after the immersion test was presented in Figure 4. The lowest remaining volume was observed for the specimen immersed in E-MEM + NBS, which agrees with the estimation based on the XRF results. In all immersion conditions, the remaining volume decreased with an increase in the immersion period, indicating the progress of the corrosion with time.

3.2.4 | Weight Loss

The weight loss per unit surface area were presented in Figure 5. The specimens immersed in E-MEM + NBS had the highest weight loss at all immersion periods. The weight loss in E-MEM + NBS drastically increased from 14 to 28 days, probably due to the occurrence of localized corrosion. At 7 days of immersion in the model tissue, the weight loss increased with increasing thickener concentration. However, after 14 or 28 days of immersion, no significant difference was observed between the weight loss in model tissue with different thickener concentrations.

3.3 | Electrochemical Test

3.3.1 | EIS

The examples of the Nyquist plot of the EIS spectra for the pure Mg specimen in the model tissue with 0.3% thickener were presented in Figure 6a. It clearly indicates the increase in the diameter of the capacitance loop with increase in the immersion period. This trend is common for the results in other

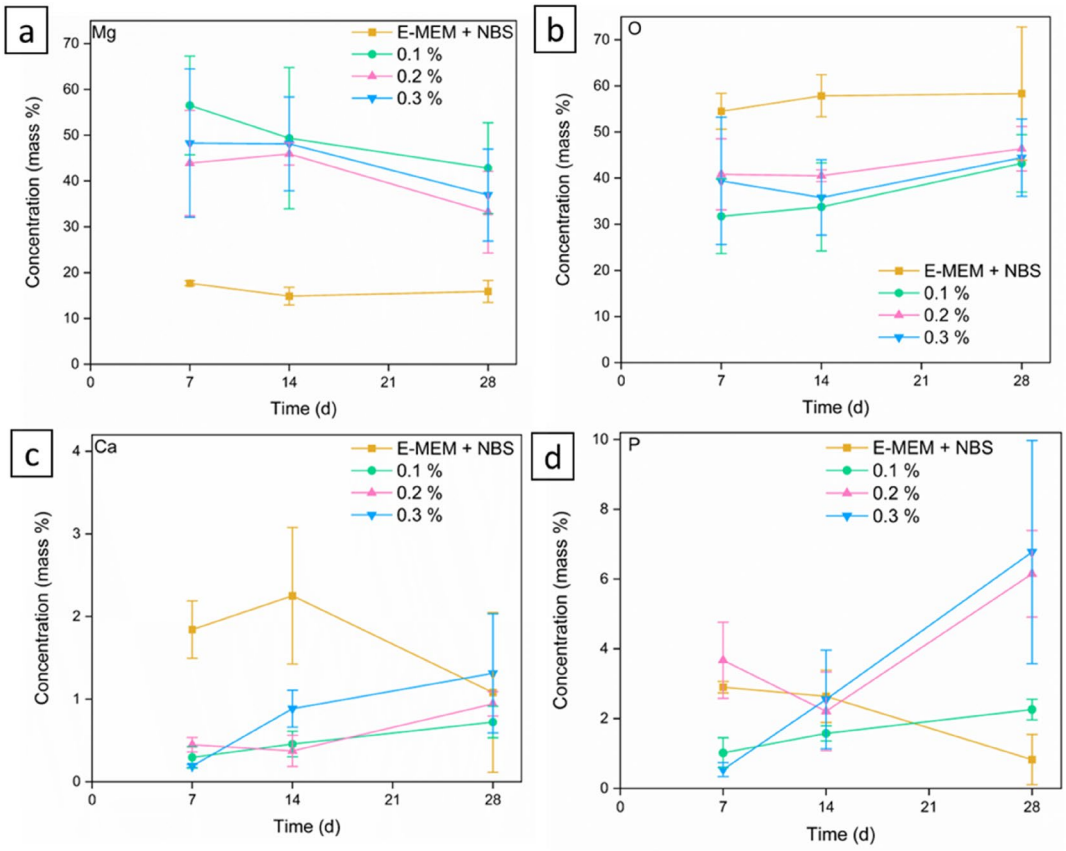

FIGURE 3 | The concentrations of (a) Mg, (b) O, (c) Ca, and (d) P from the XRF analysis of the deposited insoluble salt layer (ISL) on the pure Mg specimen surface after the immersion test ($n = 3$).

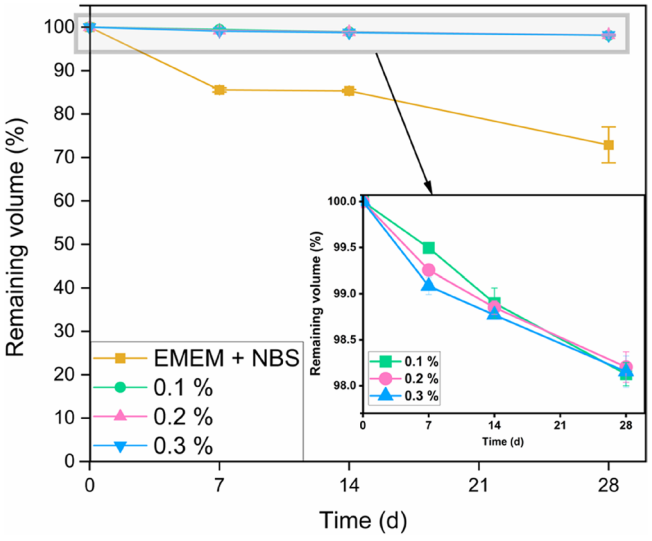

FIGURE 4 | The remaining volume of the pure Mg specimens after the immersion test ($n = 3$).

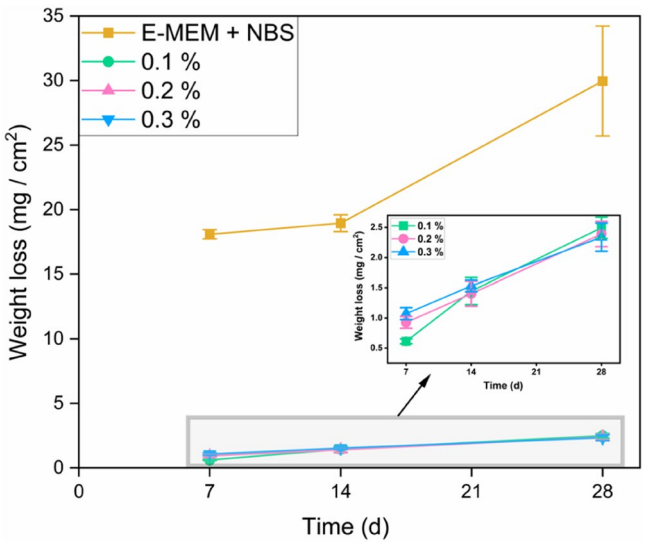

FIGURE 5 | The weight loss per unit surface area of the pure Mg specimens after the immersion test ($n = 3$).

model tissue and E-MEM + NBS. In all cases, an inductance loop was observed in the low frequency region, which can be attributed to the interference by the adsorption of insoluble salts during the EIS measurement [18, 19]. In case of the EIS spectrum with an inductance loop, the charge transfer resistance, R_{ct} has better correlation with the actual corrosion rate of a metal than the polarization resistance, R_p [20]. Figure 6b plotted R_{ct} against the immersion period which was obtained by fitting EIS data with an equivalent circuit model shown in Figure 6c. R_{ct} increased with the increase in immersion period for all the immersion conditions. For the results in the model tissue, R_{ct} increased with an increase in thickener concentration. Other parameters obtained by the fitting were shown in Table 1.

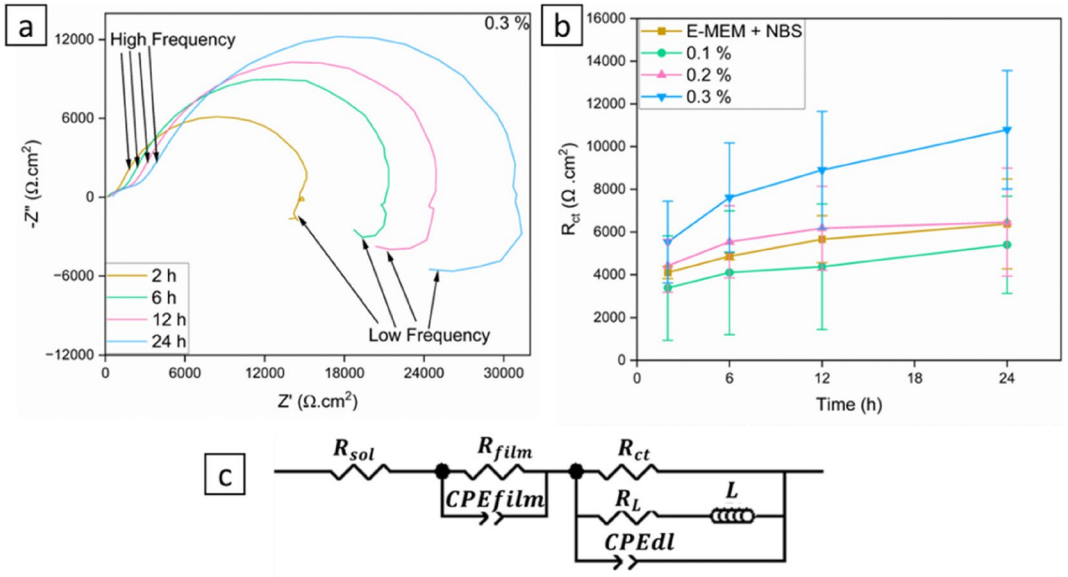

FIGURE 6 | (a) Examples of Nyquist plots of the pure Mg samples in 0.3% model tissue at different time periods, (b) R_{ct} obtained from EIS in different model tissue at different time period, and (c) the electrical equivalent circuit (EEC) used to fit the EIS spectra ($n = 3$).

3.3.2 | PDP Study

Figure 7 represents the results of PDP measurement in E-MEM + NBS and in the model tissue with 0.1%, 0.2%, and 0.3% thickener. Table 2 showed the corrosion potential (E_{corr}) and corrosion current density (I_{corr}) obtained by the Tafel method, and also pitting potential (E_{pit}) which is the potential giving the corrosion current density of 0.1 mA/cm^2. The specimens tested in the model tissue showed a decreasing trend in I_{corr} with an increase in the thickener concentration. The specimens tested with E-MEM + NBS showed the higher I_{corr} than those in model tissue, which agrees with the weight loss of the immersion test.

The SEM micrographs of the specimens after the PDP test is shown in Figure 8. There is cracked ISL observed on the specimen surface in the model tissue with thickener, whereas no cracks in the ISL were observed for E-MEM + NBS.

4 | Discussion

Mg and its alloys are considered promising biodegradable implant materials because of their high electrochemical activity. The Mg implant is corroded in the physiological environment by the following corrosion reaction:

$$Mg + 2H_2O \rightarrow Mg^{2+} + 2OH^- + H_2 \uparrow \quad (2)$$

In the physiological environment, the anodic dissolution of Mg transforms to Mg^{2+} and simultaneously the cathodic reaction resulted in the formation of hydroxide ions (OH^-) and H_2 gas. The released OH^- ions led to an increase in the pH of the physiological media and H_2 gas leads to cavity formation near to the implant surface. The corrosion of Mg depends on numerous environmental factors such as inorganic ions and organic compounds in the fluid, its pH, etc. [12, 15]. However, one of the critical environmental factors influencing the in vivo corrosion rate is the ion diffusion rate [13, 16]. In the in vivo environment, extracellular matrices and cells in the tissue modulate the diffusion of ions and gas released during Mg corrosion. In comparison to that in the physiological solution, the networks of extracellular matrices interfere the diffusion of ions, including Mg^{2+} and OH^-, resulting in the higher local pH near the specimen surface and formation of ISL on its surface. These conditions may retard the corrosion rate of Mg specimen. Wang et al. reported the fibrous tissue coverage of pure Mg wire specimen implanted into a rat aorta lumen, resulting in the lower corrosion rate and less localized corrosion (pitting) than those for in vitro static condition [13]. Bowen et al. also reported less corrosion of pure Mg coated by fibrin gel in comparison to non-coated one, giving higher tensile stress after immersion into Dulbecco's minimum essential medium (without 5%-CO_2 atmosphere) up to 21 days [21]. This can be attributed to the interference of ion diffusion by the layer of biomolecules.

Therefore, this study investigates the impact of ion diffusion on the corrosion rate of Mg. The gellan gum as a thickener with different concentrations was added to the cell culture medium to mimic the role of extracellular matrices to give different diffusion rates. Gellan gum was chosen for its ability to form a transparent gel and for its compatibility with autoclaving, ensuring sterility during experiments [16]. The thickener employed is a polysaccharide having carboxyl groups which chelate binary ions such as Ca^{2+} and Mg^{2+} in E-MEM + NBS, bridging between the thickener molecules. The higher number of thickener molecules forms more dense networks in E-MEM + NBS, resulting in the higher compression modulus (Figure 1). The dependence of the compression modulus on the thickener concentration to the power of 2.2 suggests the increase in the binding between the thickener molecules depending on its concentration. This also suggests that the higher concentration of the thickener offers more barriers on ion and gas diffusion in the model tissue, as illustrated in Figure 9c,f,i,h. The immersion and electrochemical tests were performed to evaluate the corrosion behavior of pure Mg specimen under different diffusion conditions.

TABLE 1 | Fitting results of EIS experimental data for pure Mg specimens after different exposure time in different model tissue solutions ($n = 3$).

	Time (h)	R_{sol} ($\Omega\,cm^2$)	R_{film} ($\times10^2\,\Omega\,cm^2$)	R_{ct} ($\times10^3\,\Omega\,cm^2$)	R_L ($\times10^4\,\Omega\,cm^2$)	L ($\times10^5\,H\,cm^2$)	$T_{CPEfilm}$ ($\times10^{-6}\,FS^{p-1}\,cm^2$)	$P_{CPEfilm}$	T_{CPEdl} ($\times10^{-6}\,FS^{p-1}\,cm^2$)	P_{CPEdl}	R_P ($\times10^3\,\Omega\,cm^2$)
E-MEM + NBS	2	27.0 ± 9.1	1.9 ± 0.1	4.1 ± 0.3	1.7 ± 0.7	2.7 ± 2.0	60.5 ± 24.4	0.64 ± 0.13	32.0 ± 3.5	0.74 ± 0.22	4.3 ± 0.3
	6	27.9 ± 12.4	2.7 ± 0.6	4.8 ± 0.2	1.5 ± 1.3	1.5 ± 1.0	29.8 ± 19.2	0.61 ± 0.07	35.3 ± 1.0	0.75 ± 0.20	5.1 ± 0.3
	12	24.7 ± 10.4	3.0 ± 0.7	7.1 ± 2.6	0.8 ± 0.2	1.7 ± 0.8	21.4 ± 9.5	0.62 ± 0.04	36.5 ± 2.4	0.75 ± 0.18	7.3 ± 2.4
	24	22.5 ± 10.2	3.4 ± 0.9	6.4 ± 2.1	0.6 ± 0.3	1.3 ± 1.1	31.7 ± 23.2	0.58 ± 0.07	36.8 ± 4.5	0.82 ± 0.11	6.7 ± 2.2
0.1%	2	19.3 ± 5.2	2.8 ± 0.8	3.4 ± 2.4	1.0 ± 0.9	1.6 ± 0.2	51.2 ± 7.6	0.59 ± 0.02	42.2 ± 20.5	0.86 ± 0.02	3.6 ± 2.5
	6	23.1 ± 5.8	3.6 ± 0.5	4.1 ± 2.9	0.8 ± 0.7	2.2 ± 1.0	44.1 ± 15.5	0.58 ± 0.07	47.5 ± 25.7	0.84 ± 0.04	4.4 ± 2.9
	12	25.0 ± 7.3	3.8 ± 0.5	4.3 ± 2.9	0.4 ± 0.3	2.7 ± 1.6	24.4 ± 4.0	0.60 ± 0.05	49.6 ± 26.8	0.81 ± 0.08	4.7 ± 2.9
	24	28.8 ± 10.2	3.6 ± 1.3	5.4 ± 2.3	0.7 ± 0.4	1.6 ± 0.7	15.8 ± 4.7	0.69 ± 0.08	41.0 ± 10.1	0.81 ± 0.08	5.7 ± 2.4
0.2%	2	30.1 ± 6.1	2.5 ± 1.0	4.4 ± 1.2	1.7 ± 0.4	0.4 ± 0.3	59.0 ± 16.8	0.58 ± 0.03	32.7 ± 10.7	0.86 ± 0.02	4.6 ± 1.3
	6	37.9 ± 12.9	3.5 ± 1.0	5.5 ± 1.7	2.0 ± 1.0	3.2 ± 1.7	55.3 ± 24.0	0.56 ± 0.03	32.8 ± 9.7	0.87 ± 0.02	5.8 ± 1.7
	12	50.7 ± 19.6	4.0 ± 0.8	6.2 ± 1.9	2.0 ± 0.9	2.0 ± 1.5	47.2 ± 20.9	0.56 ± 0.03	33.9 ± 8.9	0.87 ± 0.01	6.5 ± 2.0
	24	75.3 ± 31.9	4.7 ± 0.9	6.5 ± 2.5	1.3 ± 0.7	2.4 ± 0.8	37.8 ± 13.2	0.55 ± 0.04	34.4 ± 8.7	0.87 ± 0.01	6.9 ± 2.6
0.3%	2	32.7 ± 5.7	3.5 ± 0.3	5.5 ± 1.9	2.0 ± 1.2	3.3 ± 1.6	32.5 ± 12.3	0.60 ± 0.04	26.4 ± 3.6	0.87 ± 0.03	5.8 ± 1.9
	6	47.6 ± 13.2	5.6 ± 0.6	7.6 ± 2.5	1.6 ± 0.6	2.8 ± 0.7	21.6 ± 5.3	0.60 ± 0.04	25.5 ± 3.8	0.88 ± 0.03	8.2 ± 2.6
	12	74.3 ± 26.1	7.3 ± 1.0	8.9 ± 2.7	1.5 ± 0.0	2.9 ± 0.5	18.6 ± 4.2	0.59 ± 0.04	25.4 ± 4.3	0.88 ± 0.04	9.6 ± 2.7
	24	137.8 ± 59.0	9.6 ± 1.1	10.8 ± 2.8	1.5 ± 0.4	3.1 ± 0.6	16.2 ± 4.4	0.57 ± 0.05	25.4 ± 4.3	0.87 ± 0.01	11.7 ± 2.8

It has been observed that the specimens immersed in the model tissue with thickener showed lower corrosion rates than that without thickener in both the immersion and electrochemical tests. The presence of thickener impedes the diffusion of ions (Figure 9) and thereby retard the corrosion rate, resembling the situation of corrosion during the in vivo.

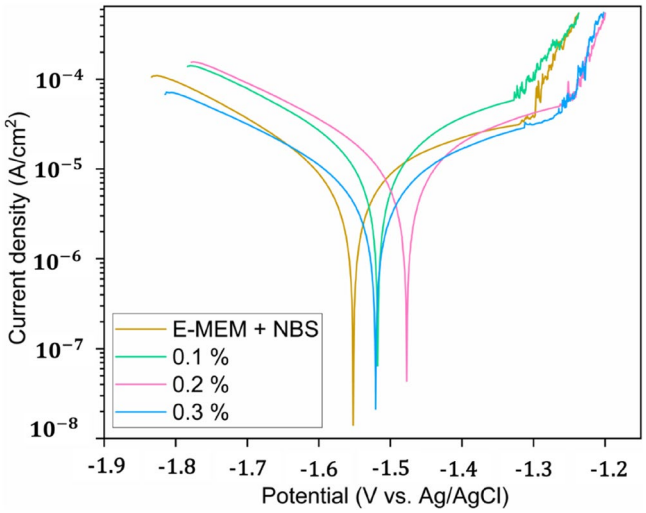

FIGURE 7 | The PDP curves of the pure Mg specimens in E-MEM + NBS and in different model tissue ($n = 3$).

The highest corrosion rate in E-MEM + NBS in immersion experiments was also confirmed from the microscopic observation (Figure 2), XRF analysis (Figure 3), and μCT analysis (Figure 4). The microscopic observation (Figure 2) shows the thick ISL on the specimen surface without thickener and the amount of ISL increased with the progress of time. The presence of pits in the specimen immersed in E-MEM + NBS after 28 days indicate the occurrence of pitting corrosion and resulted in a wide range of weight loss values (Figure 5) which is also confirmed from the remaining volume by μCT (Figure 4). This suggests that, in case of E-MEM + NBS, the occurrence and progress of localized corrosion increased the concentrations of Mg^{2+} and OH^-, giving the large amount of $Mg(OH)_2$ precipitation on the specimen surface. In other words, the ISL mainly composed by $Mg(OH)_2$ does not have an efficient protective effect against the Mg substrate corrosion. This can be confirmed by the R_{film} values in EIS analysis (Table 1); the R_{film} for E-MEM + NBS is smaller than that for 0.3% thickener, though XRF analysis indicates the thicker ISL layer (the higher O and the lower Mg percentages) for E-MEM + NBS than that for 0.3% thickener.

Regarding the effect of thickener concentrations, the corrosion rate of Mg has the decreasing trend with increase of thickener

TABLE 2 | The E_{corr}, I_{corr}, and E_{pit}, determined by the potentiodynamic polarization curve ($n = 3$).

	E-MEM + NBS	0.1%	0.2%	0.3%
E_{corr} (V)	−1.55 ± 0.01	−1.54 ± 0.04	−1.47 ± 0.05	−1.53 ± 0.03
I_{corr} (μA/cm²)	17.99 ± 3.70	20.25 ± 3.13	16.46 ± 3.57	12.57 ± 3.09
E_{pit} (V)	−1.28 ± 0.01	−1.34 ± 0.05	−1.21 ± 0.05	−1.32 ± 0.09

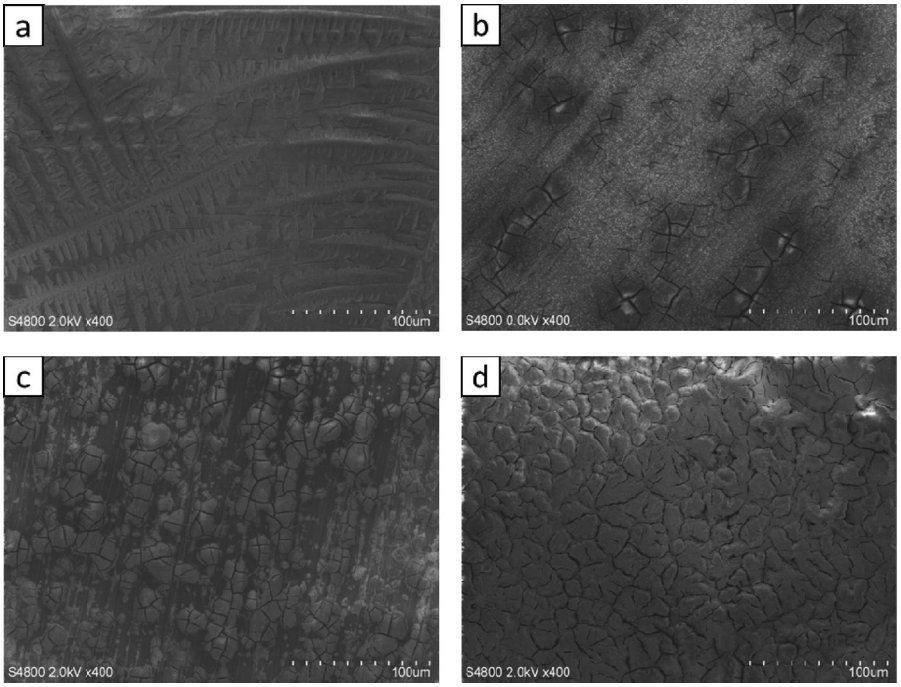

FIGURE 8 | The SEM observation of the pure Mg specimens after the electrochemical test in (a) E-MEM + NBS, (b) 0.1%, (c) 0.2%, and (d) 0.3% model tissue ($n = 3$).

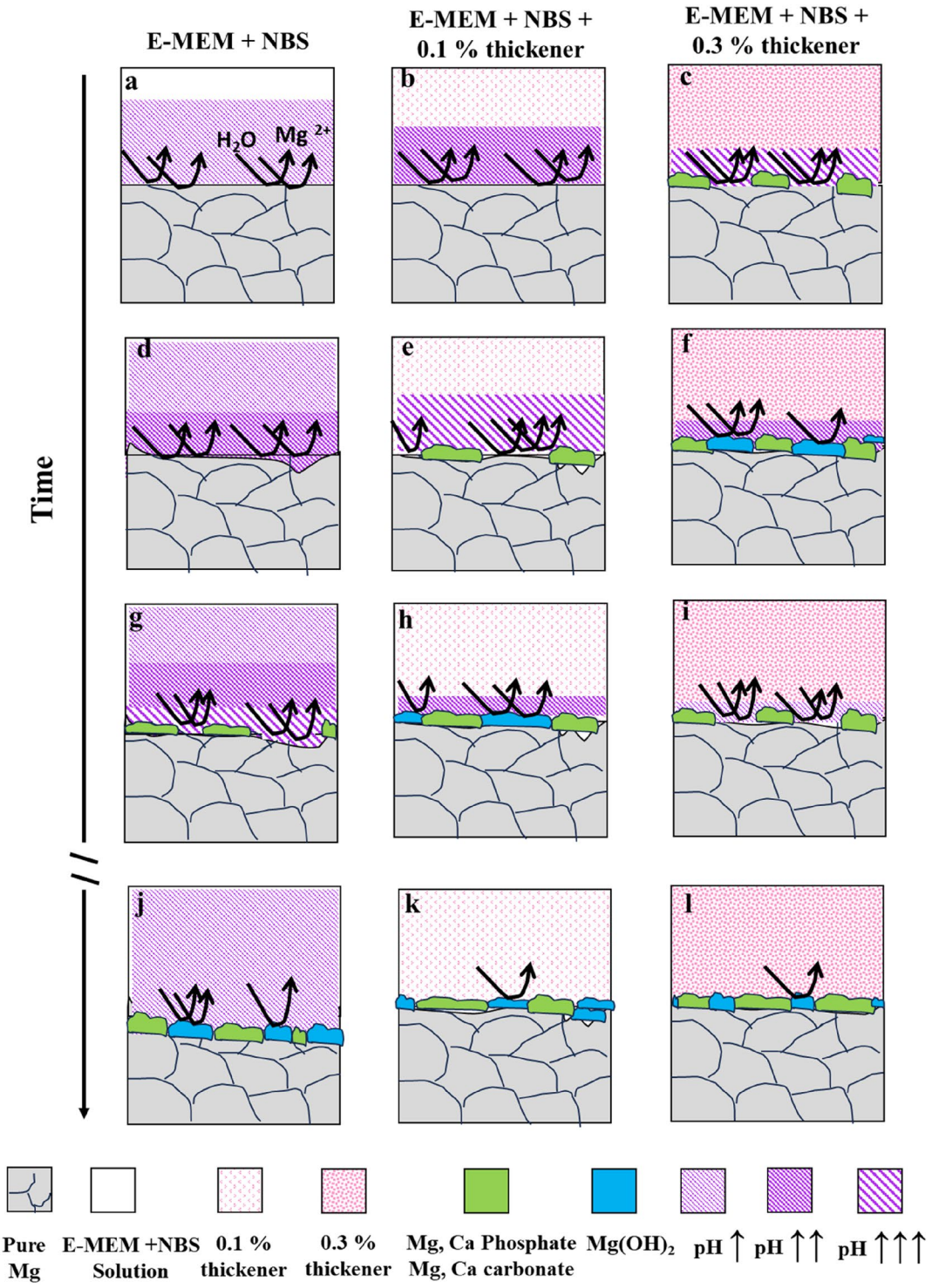

FIGURE 9 | Schematic representation of the progress of corrosion process of pure Mg in E-MEM + NBS solution (a, d, g, and j), model tissue with low (0.1%) (b, e, h, and k) and high (0.3%) (c, f, i, and l) concentration of thickener. The arrow indicates Mg corrosion reaction. In case of 0.3% thickener, the initial corrosion reaction resulted in the higher local pH near the specimen surface (c) than 0.1% thickener concentration (b) or E-MEM + NBS (a), encouraging insoluble salt layer formation including calcium/magnesium phosphate and carbonate in the earlier stage of immersion. Due to the limited supply of calcium, carbonate and phosphate ions from offshore by low diffusion rate, $Mg(OH)_2$ will be dominant for the precipitation on the specimen surface (f). The ISL formation retards the corrosion of the substrate, and then the local pH eventually recovers to close to neutral, dissolving the $Mg(OH)_2$ (i). This slightly increases the substrate corrosion, which increases the local pH and encourages ISL formation (l). In case of 0.1% thickener, pH fluctuation will be milder than 0.3% thickener.

concentration in the model tissue after 28 days of immersion. The same trend was also confirmed by EIS and PDP tests (Tables 1 and 2). In our previous study, we demonstrated through solubility limit calculations that diffusion in a corrosive environment affects the composition of ISL precipitating on the Mg surface by altering the local ion concentrations near the surface

[17]. The EIS analysis also suggests the different nature of the ISL on the specimen surface; the R_{film} has the increasing trend with increase in immersion time, which is more obvious at 0.3% thickener than 0.2% or 0.1% thickener. This result indicates the involvement of the diffusion process in the model tissue for the behavior of ISL formation along with substrate Mg corrosion.

Figure 9 illustrates the schematic representation of the progress of corrosion process of pure Mg in model tissue with low (0.1%) [Figure 9b,e,h,k] and high (0.3%) [Figure 9c,f,i,l] concentrations of thickener in comparison to E-MEM + NBS solution [Figure 9a,d,g,j]. Altghough the rate of corrosion reaction are similar in all the media immediate after the immersion of the pure Mg, the precipitates of Mg and/or Ca phosphate/carbonate were deposited on the surface of the specimen immersed in 0.3% thickener which attributed due to rapid pH change, [Figure 9c], whereas no deposition were observed in E-MEM + NBS solution [Figure 9a] and 0.1% thickener [Figure 9b]. With progress of time, the pH in 0.3% thickener decreases and $Mg(OH)_2$ deposited [Figure 9f] and lowered the corrosion reaction because of surface passivation. Again $Mg(OH)_2$ starts to dissolve with further lower in pH because of its instability at lower pH and corrosion reaction accelerates because of exposure of the specimen surface to the model tissue [Figure 9i]. Similar steps were also observed in E-MEM + NBS solution, and 0.1% thickener with delay of the deposit of the precipitates of Mg and/or Ca phosphate/carbonate. Furthermore, with long immersion period, corrosion rate decreases in all the media, but the corrosion rate achieved by immersion of the specimen in model tissue are in the close range to that of in vivo.

Table 3 summarize the corrosion rates of pure Mg after 7 days of immersion in comparison with in vivo results in literatures. In the present study, the corrosion rates after 7 days of immersion were 5.43 ± 0.10, 0.18 ± 0.01, 0.28 ± 0.03, 0.32 ± 0.03 mm/y for the E-MEM + NBS and the model tissue with 0.1%, 0.2%, and 0.3% thickener, respectively. Myrissa et al. reported a corrosion rate of pure Mg pins as 0.40 mm/y by implantation in the femoral bone of rats for 7 days [10]. Walker et al. also reported a corrosion rate of pure Mg pins as 0.390 mm/y by implantation into the subcutaneous tissue of rabbits for 7 days [9]. These in vivo values are close to those obtained in the model tissue at 0.2% or 0.3% thickener. However, for the same period, the *in vitro* immersion test in MEM + 40 g/L bovine serum albumin [9] and Nor's solution (CO_2—bicarbonate buffered Hanks' solution) [22] showed the corrosion rates of 2.185 and 3.22 mm/y, respectively. This indicates the poor correlation between the published results with in vitro models and *in vivo* behavior, which is also summarized by Staiger et al. [24]. In the current study, we demonstrated that the use of thickeners such as gellan gum can be more reliable in vitro models to predict in vivo corrosion rates, potentially reducing the need for animal testing and elucidating the underlying mechanisms. The model system can be applied for both electrochemical and immersion tests, which can give essential results for accurate prediction of the corrosion behavior. Another advantage of the model tissue is controllability of the diffusion rates and other properties in the tissue by changing the thickener and its concentration, which enables to simulate the various types and states of the tissues.

Although the addition of thickener to cell culture medium offers a better in vitro model system and allows understanding of the diffusion rate on the Mg corrosion, it has a limit to fully simulate the degradation behavior of Mg implants in clinical application. In clinical cases, the degradation behavior of Mg implants can be influenced by various factors such as implantation sites [25] as well as individuals' conditions such as age, underlying diseases, pathological mechanisms, etc. Furthermore, most of these clinical, pathological factors are difficult to recreate in the *in vivo* models. However, the model tissue system developed in our study can be improved to simulate these clinical factors in combination with other techniques such as microflow systems and tissue engineering. The in vitro model system with pathological tissue simulation can be useful for the elucidation of undermining mechanism in pathological conditions, contributing to the development of new clinical treatments and medical devices.

TABLE 3 | Comparison of the corrosion rates of pure Mg for 7 days of in vitro immersion or in vivo implantation.

	Environment	Corrosion rate (mm/y), (After 7 days)	References
In vitro	E-MEM + NBS	5.43 ± 0.10	Current study
	Model tissue with 0.1% thickener	0.18 ± 0.01	
	Model tissue with 0.2% thickener	0.28 ± 0.03	
	Model tissue with 0.3% thickener	0.32 ± 0.03	
	MEM + 40 g/L bovine serum albumin	2.185	[9]
	Nor's solution (CO_2-bicarbonate buffered Hanks' solution)	~3.22	[22]
	Simulated body fluid (SBF)	1.33 ± 0.23	[23]
in vivo	Implantation (rat, subcutaneous tissue)	0.390	[9]
	Implantation (rat, femoral bone)	0.40	[10]

5 | Conclusions

In this study, we successfully developed the model tissue with different diffusion rates to analyze the influence of ion diffusion on Mg corrosion. The thickener with appropriate concentrations

was added to the cell culture medium (E-MEM + NBS) to form the model tissue with different diffusion rates. The increased concentrations of the thickener resulted in increased modulus, suggesting more bindings between the thickener molecules to be diffusion barriers. Pure Mg specimens immersed in the medium without thickener exhibited the highest corrosion rate in both immersion and electrochemical tests. There is an impediment of ion diffusion in the model tissue with increased thickener concentrations, thereby decreasing the corrosion rate. The corrosion rate obtained by the model tissue with 0.2%–0.3% thickener lies in the range of reported in vivo results. These findings suggest that the developed model can effectively investigate the biodegradation behavior of Mg, providing valuable insights into the mechanisms and controlling factors of Mg corrosion in biological environments.

Acknowledgments

This work was partially supported by JSPS KAKENHI Grant number JP22H03988 and by ARIM of MEXT(JPMXP1223NM5415). We thank Ms. Akemi Kikuta from the National Institute of Materials Science for the technical support.

Conflicts of Interest

The authors declare no conflicts of interest.

Data Availability Statement

The data that support the findings of this study are available on request from the corresponding author. The data are not publicly available due to privacy or ethical restrictions.

References

1. S. Virtanen, "Biodegradable mg and mg Alloys: Corrosion and Biocompatibility," *Materials Science and Engineering B* 176, no. 20 (2011): 1600–1608, https://doi.org/10.1016/j.mseb.2011.05.028.

2. M. Mohammadi Zerankeshi, R. Alizadeh, E. Gerashi, M. Asadollahi, and T. G. Langdon, "Effects of Heat Treatment on the Corrosion Behavior and Mechanical Properties of Biodegradable Mg Alloys," *Journal of Magnesium and Alloys* 10, no. 7 (2022): 1737–1785, https://doi.org/10.1016/j.jma.2022.04.010.

3. N. W. Alcock, I. Macintyre, and I. Radde, "Concentration of Magnesium in Human Plasma or Serum," *Nature* 206, no. 4979 (1965): 89–90, https://doi.org/10.1038/206089a0.

4. P. Chakraborty Banerjee, S. Al-Saadi, L. Choudhary, S. E. Harandi, and R. Singh, "Magnesium Implants: Prospects and Challenges," *Materials* 12, no. 1 (2019): 136, https://doi.org/10.3390/ma12010136.

5. M. R. Sahu, T. S. Sampath Kumar, U. Chakkingal, V. K. Dewangan, and M. Doble, "Influence of Fine-Grained Structure Produced by Groove Pressing on the Properties of Pure Mg and Commercial ZE41 Alloy," *Journal of Biomedical Materials Research. Part A* 111, no. 8 (2023): 1161–1175, https://doi.org/10.1002/jbm.a.37502.

6. D. Noviana, D. Paramitha, M. F. Ulum, and H. Hermawan, "The Effect of Hydrogen Gas Evolution of Magnesium Implant on the Postimplantation Mortality of Rats," *Journal of Orthopaedic Translation* 5 (2016): 9–15, https://doi.org/10.1016/j.jot.2015.08.003.

7. K. Chen, X. Xie, H. Tang, et al., "In Vitro and In Vivo Degradation Behavior of Mg–2Sr–Ca and Mg–2Sr–Zn Alloys," *Bioactive Materials* 5, no. 2 (2020): 275–285, https://doi.org/10.1016/j.bioactmat.2020.02.014.

8. I. Antoniac, R. Adam, A. Biță, et al., "Comparative Assessment of In Vitro and In Vivo Biodegradation of Mg-1Ca Magnesium Alloys for Orthopedic Applications," *Materials* 14, no. 1 (2020): 84, https://doi.org/10.3390/ma14010084.

9. J. Walker, S. Shadanbaz, N. T. Kirkland, et al., "Magnesium Alloys: Predicting In Vivo Corrosion With In Vitro Immersion Testing," *Journal of Biomedical Materials Research. Part B, Applied Biomaterials* 100B, no. 4 (2012): 1134–1141, https://doi.org/10.1002/jbm.b.32680.

10. A. Myrissa, N. A. Agha, Y. Lu, et al., "In Vitro and In Vivo Comparison of Binary Mg Alloys and Pure mg," *Materials Science and Engineering: C* 61 (2016): 865–874, https://doi.org/10.1016/j.msec.2015.12.064.

11. A. H. M. Sanchez, B. J. C. Luthringer, F. Feyerabend, and R. Willumeit, "Mg and Mg Alloys: How Comparable are In Vitro and In Vivo Corrosion Rates? A Review," *Acta Biomaterialia* 13 (2015): 16–31, https://doi.org/10.1016/j.actbio.2014.11.048.

12. A. Atrens, S. Johnston, Z. Shi, and M. S. Dargusch, "Viewpoint – Understanding Mg Corrosion in the Body for Biodegradable Medical Implants," *Scripta Materialia* 154 (2018): 92–100, https://doi.org/10.1016/j.scriptamat.2018.05.021.

13. J. Wang, L. Liu, Y. Wu, et al., "Ex Vivo Blood Vessel Bioreactor for Analysis of the Biodegradation of Magnesium Stent Models With and Without Vessel Wall Integration," *Acta Biomaterialia* 50 (2017): 546–555, https://doi.org/10.1016/j.actbio.2016.12.039.

14. K. X. Kuah, S. Wijesinghe, and D. J. Blackwood, "Toward Understanding In Vivo Corrosion: Influence of Interfacial Hydrogen Gas Build-Up on Degradation of Magnesium Alloy Implants," *Journal of Biomedical Materials Research. Part A* 111, no. 1 (2023): 60–70, https://doi.org/10.1002/jbm.a.37446.

15. S. Kumar, P. Katyal, R. N. Chaudhary, and V. Singh, "Assessment of Factors Influencing Bio-Corrosion of Magnesium Based Alloy Implants: A Review," *Materials Today Proceedings* 56 (2022): 2680–2689, https://doi.org/10.1016/j.matpr.2021.09.262.

16. A. Yamamoto and A. Kikuta, "Development of a Model System for Gas Cavity Formation Behavior of Magnesium Alloy Implantation," *ACS Biomaterials Science & Engineering* 8, no. 6 (2022): 2437–2444, https://doi.org/10.1021/acsbiomaterials.1c01429.

17. M. Hayashi, A. Yamamoto, T. Aizawa, Y. Yusa, Y. Shimizu, and Y. Imai, "In Vitro Analysis of Insoluble Salt Formation Mechanism Associated With Mg Corrosion—Variations Depending on the Diffusion Environment in Model Tissue," *Biomedical Materials* 19, no. 2 (2024): 025010, https://doi.org/10.1088/1748-605X/ad1d7f.

18. Y. Song, D. Shan, R. Chen, and E.-H. Han, "Corrosion Characterization of Mg–8Li Alloy in NaCl Solution," *Corrosion Science* 51, no. 5 (2009): 1087–1094, https://doi.org/10.1016/j.corsci.2009.03.011.

19. Y. Song, D. Shan, and E.-H. Han, "A Novel Biodegradable Nicotinic Acid/Calcium Phosphate Composite Coating on Mg–3Zn Alloy," *Materials Science and Engineering: C* 33, no. 1 (2013): 78–84, https://doi.org/10.1016/j.msec.2012.08.008.

20. M. Itagaki, M. Imamura, A. Taya, and K. Watanabe, "Corrosion Resistance of Electrochemical Impedance With Inductive Behavior," *Zairyo-to-Kankyo* 50, no. 9 (2001): 400–402, https://doi.org/10.3323/jcorr1991.50.400.

21. P. K. Bowen, J. A. Gelbaugh, P. J. Mercier, J. Goldman, and J. Drelich, "Tensile Testing as a Novel Method for Quantitatively Evaluating Bioabsorbable Material Degradation," *Journal of Biomedical Materials Research. Part B, Applied Biomaterials* 100B, no. 8 (2012): 2101–2113, https://doi.org/10.1002/jbm.b.32775.

22. N. I. Zainal Abidin, B. Rolfe, H. Owen, et al., "The In Vivo and In Vitro Corrosion of High-Purity Magnesium and Magnesium Alloys WZ21 and AZ91," *Corrosion Science* 75 (2013): 354–366, https://doi.org/10.1016/j.corsci.2013.06.019.

23. Y. Wang, Y. H. He, Z. J. Zhu, et al., "In Vitro Degradation and Biocompatibility of Mg-Nd-Zn-Zr Alloy," *Chinese Science Bulletin* 57, no. 17 (2012): 2163–2170, https://doi.org/10.1007/s11434-012-5066-6.

24. M. P. Staiger, F. Feyerabend, R. Willumeit, et al., "Summary of the Panel Discussions at the 2nd Symposium on Biodegradable Metals, Maratea, Italy, 2010," *Materials Science and Engineering B* 176, no. 20 (2011): 1596–1599, https://doi.org/10.1016/j.mseb.2011.09.032.

25. D. Zhao, F. Witte, F. Lu, J. Wang, J. Li, and L. Qin, "Current Status on Clinical Applications of Magnesium-Based Orthopaedic Implants: A Review From Clinical Translational Perspective," *Biomaterials* 112 (2017): 287–302, https://doi.org/10.1016/j.biomaterials.2016.10.017.

Supporting Information

Additional supporting information can be found online in the Supporting Information section.